

Scattering of knotted vortices (Hopfions) in the Faddeev-Skyrme model

J. Hietarinta^{1*}, J. Palmu¹, J. Jäykkä^{1,2} and P. Pakkanen¹

¹ Department of Physics and Astronomy, University of Turku,
FI-20014 Turku, Finland

² School of Mathematics University of Leeds,
LS2 9JT Leeds, United Kingdom

Abstract

Several materials, such as ferromagnets, spinor Bose-Einstein condensates, and some topological insulators, are now believed to support knotted structures. One of the most successful base-models having stable knots is the Faddeev-Skyrme model and it is expected to be contained in some of these experimentally relevant models. The taxonomy of knotted topological solitons (Hopfions) of this model is known. In this paper we describe some aspects of the dynamics of Hopfions and show that they do indeed behave like particles: during scattering the Hopf charge is conserved and bound states are formed when the dynamics allows it. We have also investigated the dynamical stability of a pair of Hopfions in stacked or side-by-side configurations, whose theoretical stability has been recently discussed by Ward.

1 Introduction

1.1 Background

Topological solitons play an important role in many areas of physics. They can be beneficial, like the Abrikosov vortices in type II superconductors or unwanted like the dislocations in nematic liquid crystals. Likewise, the creation and observation of topological solitons in Bose-Einstein condensates is nowadays routine in laboratories around the world. Recent experimental observations have renewed interest in the types of models that can support topological solitons, and it is important to understand the basic properties and phenomenology of topological solitons in these models. Theoretically, the possibility of the presence of skyrmion structures in certain materials has been known for long[1, 2]

*corresponding author, e-mail: hietarin@utu.fi

(for a more recent work and references, see [3]), and this has recently been experimentally verified at least in MnSi[4] and $\text{Fe}_{1-x}\text{Co}_x\text{Si}$ [5]. A newer theoretical discovery is the family of materials collectively known as topological insulators (for a review, see [6]). The experimental observation of topological insulator phase in $\text{Bi}_{1-x}\text{Sb}_x$ [7], Bi_2Se_3 [8] and Bi_2Te_3 [9] confirmed these theoretical predictions and served to further add relevance to the basic research involving topological solitons. For the present work, perhaps the most interesting possibility is the discovery that frustrated magnetic materials may support topological insulator phases, where the wave-function in momentum-space is classified by the Hopf invariant[10]. As will be discussed below, when the system is described by the Hopf charge, it will support knotted structures.

Knotted structures have a long history in physics. They were first considered by Lord Kelvin, who proposed in 1867 [11] that atoms could be knotted tubes of ether. This idea did not yield a satisfactory atomic theory, but subsequently more realistic models have been proposed with potential for knotted structures. This has been done, for example, in the context of ferromagnets[12], Bose-Einstein condensates[13], and optics[14]. A unifying feature of all these, in addition to the knotted structures, is that all these phenomena and their knots can be described by classical field theory.

1.2 Hopf charge

In a field theoretical description the knot is not made of a rope in empty space but through the twisting of a globally defined vector field. Here we will only consider the case in which the knottedness is characterized by the Hopf charge. The minimal model with stable knotted structures seems to be the Faddeev-Skyrme model [15] and it is believed that this model is contained within various models with immediate physical application, such as the two-component Ginzburg-Landau model modified with an additional Ward like term. [16].

The physical carrier field in the Faddeev-Skyrme model is a smooth 3D unit vector field $\phi = (\phi_1, \phi_2, \phi_3)$ with $\phi(\mathbf{x}) \cdot \phi(\mathbf{x}) = 1$. Unit vector fields with such properties have been proposed to exist, e.g., in super-fluid ^3He in its A-phase (Continuous Unlocked Vortex)[17] and in ferromagnets[12]. In order to be able to define the Hopf charge it is also necessary that the vector field ϕ approaches the same value at all asymptotic directions: $\phi(\mathbf{x}) \rightarrow \phi_\infty$, when $|\mathbf{x}| \rightarrow \infty$ (asymptotic triviality). Asymptotic triviality means that from the point of view of ϕ the Euclidean space R^3 is topologically like the sphere S^3 and this allows one to define the Hopf charge as an element of the homotopy class $\pi_3(S^2) = \mathbb{Z}$. A concrete

Hopfion vortex ring with Hopf charge $Q = -1$ is given by

$$\phi = \left(\frac{4(2xz - y(r^2 - 1))}{(1 + r^2)^2}, \frac{4(2yz + x(r^2 - 1))}{(1 + r^2)^2}, \frac{8(r^2 - z^2)}{(1 + r^2)^2} - 1 \right), \quad (1)$$

where $r^2 = x^2 + y^2 + z^2$, however, this configuration is not a solution for the equation of motion studied here. It is easy to see that $\phi = (0, 0, -1)$ at infinity in any direction and also on the z -axis, while the preimage of $\phi = (0, 0, +1)$, which is defined as the vortex core, is the ring $x^2 + y^2 = 1, z = 0$.

Since the core is just a simple loop it does not explain the Hopf charge. For that purpose we need to consider also the preimage-curve of some other value of ϕ and the linking of these two curves. Let us for example consider the tubular iso-surface defined by $\phi_3 = \frac{4}{5}$ and on it the curve that is the preimage of $\phi = (\frac{3}{5}, 0, \frac{4}{5})$, see Figure 1. The linking number of this curve with the core-line can now be computed using the standard rules of knot theory: If the top arrow can be aligned with the bottom arrow using a clockwise rotation, the crossing is assigned -1 , for a counterclockwise rotation $+1$. The linking number is then $1/2$ of the sum of signed crossings. From Figure 1 we can see that there are two crossings of signature -1 and therefore the Hopf charge is $Q = -1$.

The Hopf charge can also be computed by integrating a charge density: For the antisymmetric field $F_{ij} := \phi \cdot \partial_i \phi \times \partial_j \phi$ one constructs the potential A_i such that $F_{ij} = \partial_i A_j - \partial_j A_i$ and then the Hopf charge is given by

$$Q = \frac{1}{32\pi^2} \int \epsilon^{ijk} A_i F_{jk} d^3x. \quad (2)$$

A proof that these two methods give the same result is given in [18].

1.3 The dynamics

For the dynamics we use a variation of the Skyrme model as proposed by Faddeev in 1975[15], it is defined by the Lagrangian

$$L = \int [(\partial_\mu \phi)^2 + g F_{\mu\nu}^2] d^3x, \quad F_{\mu\nu} := \phi \cdot \partial_\mu \phi \times \partial_\nu \phi. \quad (3)$$

Note that in the static case we have the following scaling property: under the scaling $r \rightarrow \lambda r$ the integrated kinetic term scales as λ while the integrated F^2 term scales as λ^{-1} . Thus according to the virial theorem nontrivial configurations will attain some fixed size determined by the *dimensional* coupling constant g . In the computations reported below we used $g = 1/2$.

A very important property of this model is that the energy is bounded from below[19] and from above[20]

$$h' |Q|^{\frac{3}{4}} \leq E \leq h |Q|^{\frac{3}{4}}, \quad (4)$$

where h, h' are some constants and Q the Hopf charge. Since the exponent of the charge is less than 1 it follows that configurations with higher Hopf charge tend to form bound states rather than split into several charge 1 states.

An intriguing question is the form of the minimum energy states with higher Hopf charge. After some tentative works[21, 22] detailed taxonomy has been obtained by Battye and Sutcliffe[23, 24, 25] and Hietarinta and Salo[26, 27]. The results follow very well[27, 25] the bound (4). It turns out that a twisted torus-like configuration (similar to (1)) is a minimum energy state only for $|Q| \leq 4$ [27], for higher charges linked or knotted configurations are found. The trefoil knot is persistently found for charge $|Q| = 7$ from a wide variety of initial states, even for long vortices.[28]

We will next give the computational method and then describe the results for two dynamical studies: scattering head on collisions, and attractive and repulsive channel simulations inspired by the work of Ward in [29].

2 Computational method

For scattering dynamics we used the Lagrangian (3) in the full 3+1-dimensional Minkowski space-time (with $c = 1$) and the resulting Euler-Lagrange equations, derived with a Lagrange multiplier to guarantee $\phi \cdot \phi = 1$ during evolution. The second order (in time) equation was split into two first order equations for numerical computations. The spatial derivatives are discretized on 5^3 points. The formulae are quite similar to those in [30]. Time evolution was computed using 4th order Runge-Kutta (five stage low memory version[31]). For scattering studies the computational lattice varied between 200^3 and 300^3 , but all the simulations used the same lattice constant $h = 0.15$. In the three-Hopfion collisions the physical size of the grid was $45.0 \times 30.0 \times 30.0$ and in the double-collisions 30.0^3 . The constant of Courant-Friedrichs-Lewy like condition linking time and space discretization is $c_{fl} \equiv \Delta t/h = 0.02$. Ward's channel simulations were computed in a lattice of 300^3 unless otherwise noted; the grid constant was still $h = 0.15$ but $c_{fl} = 0.2$. The Courant instability was controlled by smoothing. For computational platform we used SAMRAI[32].

As our work progressed the significance of boundary condition became more and more clear and thus we have tried a variety of different methods and parameter configurations to minimize boundary errors. The presented two- and three-Hopfions scatterings are calculated with Dirichlet boundary conditions $\phi|_{\partial} = \phi_{\infty} = (0, 0, -1)$, and the Ward's channel simulations with Neumann boundary condition $\partial_{\{x,y,z\}}\phi|_{\partial} = (0, 0, 0)$. Furthermore, in the two- and three-Hopfion scatterings we had a thin and mild absorption layer near

the boundary in order to prevent radiation from reflecting and re-entering the scattering region.

Visualization of a vector field is problematic. Since we cannot plot the vector field at all points of the 3D space we chose to plot iso-surfaces determined by the value of the third component ϕ_3 , often with $\phi_3 = 0.7$, which is a narrow tube around the core. This tube is painted[26] with color determined by the first two components of ϕ . For visualization platform we used VisIt[33].

3 Results

3.1 The fundamental deformation processes

Before analyzing specific scattering processes it is important to recall the possible elementary deformation processes. It was already noted above that it is not enough to consider only the core-line but also how the unit-vector field twists around it. In fact, the proper knot theoretical setting is to use *framed links* which can be realized as *directed ribbons* (pre-images of line segments[34]). This adds local information near the curve, e.g., twisting around it. Knot deformations correspond to ribbon deformations, which allow certain types of crossing and breaking, in which the Hopf charge will nevertheless be conserved. Examples of ribbon deformations can be seen in[34].

3.2 Collisions and scattering

We will now consider the scattering of low-charge “un-knot” Hopfions in two different situations: three-body scattering on a fixed target with projectiles from left and right, and two-body scattering with impact parameter. The the individual Hopfions (minimum energy states) were first created using the steepest descent method (corresponding to 1st order dissipative dynamics with a fictitious time) [26]. These Hopfions were then rotated, Lorentz boosted and combined to form the initial configurations for scattering. This was done using interpolation routines provided by the SciPy python library.

In the first scattering process, for which snapshots are given in Figure 2, with full details in Movie S1, we have two charge $Q = -2$ Hopfions approaching a stationary $Q = -3$ target head on, from left and right. The moving Hopfions were Lorentz boosted numerically to speeds 0.75 and -0.75 , respectively, and then immersed into the computational box. Since the total charge is $Q = -7$ we expect the result to be a trefoil knot. This is indeed the case, after several intermediate steps. The resulting trefoil is not stationary but rather oscillates and rotates, and eventually the Hopfion settles down drifting slowly. Since $7^{3/4}/(2 \cdot 2^{3/4} + 3^{3/4}) \approx 0.76$ there is theoretically 24% excess energy, some of which

will radiate as low amplitude, close to vacuum ($\phi_3 \approx -1$), waves from the scattering region. These are not visible at the iso-surface $\phi_3 = 0.7$ level. The resulting drift is probably due to momentum conservation in an asymmetric radiation background.

In Figures 3,4 (for details see Movies S2 and S3) we have a situation similar to the one in Figure 2, except that now the central target has charge $Q = +3$. The total charge is then $Q = -1$ and indeed the final state has one Hopfion of $Q = -1$. As the Hopfions approach each other they deform by the rule “like colors attract”, thereby preparing for ribbon crossings. Since $1/(2 \cdot 2^{3/4} + 3^{3/4}) \approx 0.18$ most of the energy has to radiate away. This can be clearly seen in Figure 4 (Movie S3) which describes in further detail the later stages of the process. In this figure we have indicated the distribution of energy density by a white cloud. Up to $t = 20.1$ the energy is localized near the vortex tube but when the deformation towards $Q = -1$ continues more radiation is released and can be seen to radiate away.

For the two-body scattering with impact parameter we present the scattering of two $Q = -3$ Hopfions with two different impact parameters. In Figure 5 (Movie S4) we have the impact parameter 3.75 and the Hopfions have speed 0.5. Although the Hopfions touch briefly at $t = 12$ the speed and distance prevent a bound state from forming. The individual Hopfions just continue tumbling along a slightly bent trajectory.

For the same speeds but with slightly smaller impact parameter value 3.6 the result is entirely different (Figure 6, Movie S5). For a moment it seems that the Hopfions would again continue along their individual trajectories but there is just enough time to form an elongated loop. After this the evolution is typical for the total charge $|Q| = 6$ case: The loop behaves like an over-twisted rubber band and proceeds to make one ribbon crossing deformation to reach the linked loop configuration that is standard for this Hopf charge. The linked configuration continues to rotate and oscillate.

The above results illustrate the difficulty associated with trying to make any generalizations about the behavior of Hopfions. However, some progress has been made by modeling Hopfions with elastic rods[35]. It would be interesting to see if the elastic rod model could be extended to approximate dynamical features as well.

3.3 Static initial states

We will next consider the case of two unit charge Hopfion unknots placed on static positions not too far from each other. This case was studied by Ward [29], who observed (using energy minimization) that under symmetry preserving relaxation an axisymmetric two Hopfion state reaches a local minimum ($E = 2.26$) where the soliton cores around the symmetry axis are separated by a nonzero but finite distance. He also noticed that this

separated configuration has 13% higher total energy than the twice wound multisoliton state ($E = 2.00$) both of which are in the same homotopy class. The nature of the axisymmetric state is not yet clear and, as Ward stated, more study is needed to investigate whether the state is actually a local minimum or just a saddle-point.

For these cases we prepared the initial states using Wards proposal, that in the stereographic coordinates $W = (\phi_1 - i\phi_2)/(1 + \phi_3)$, a good ansatz for a $|Q| = 1$ Hopfion is given by $W = (x + iy)/(z - if(r))$, where $r = (x^2 + y^2 + z^2)^{1/2}$ and f is some specific function of r (see Equation (4) in [29], Ward uses $W = (\phi_1 + i\phi_2)/(1 + \phi_3)$). Actually this can be generalized by adding some signs in the expression:

$$W = \frac{\sigma_1 x + i\sigma_2 y}{z - i\tau\sigma_1\sigma_2 f(r)}. \quad (5)$$

Here the sign of τ determines whether this is a Hopfion or anti-Hopfion, while the signs of the σ 's can be changed by 180° rotations around one of the coordinate axes. Thus for a single Hopfion the signs σ_i are irrelevant but they do play a role when we construct an initial state with two Hopfions. ¹

3.3.1 Stacked Hopfions

It was noted by Ward [29] that a good two Hopfion ansatz is obtained just by adding the corresponding W functions (5). Thus for the case with two Hopfions located at $z = \pm a$ and sharing the same axis (Ward's Channel A) we can take

$$W = \frac{\sigma_1 x + i\sigma_2 y}{z - a - i\tau\sigma_1\sigma_2 f(r_{z-a})} + \frac{\sigma'_1 x + i\sigma'_2 y}{z + a - i\tau\sigma'_1\sigma'_2 f(r_{z+a})}, \quad (6)$$

as the starting configuration. Here $r_{z\pm a} = (x^2 + y^2 + (z \pm a)^2)^{1/2}$.

Ward uses a dipole pair to describe the configuration, in our notation $P_+ = (\sigma_1, 0, 0)$, $Q_+ = (0, \sigma_2, 0)$ and $P_- = (\sigma'_1, 0, 0)$, $Q_- = (0, \sigma'_2, 0)$, so that $D_+ := P_+ \times Q_+ = (0, 0, \sigma_1\sigma_2)$, etc. Furthermore the angle between P_+ and P_- is 0 if $\sigma_1 = \sigma'_1$ and 180° if $\sigma_1 = -\sigma'_1$.

The signs in (6) can be changed by various 180° rotations and this way the 16 possible sign combinations $(\sigma_1, \sigma_2, \sigma'_1, \sigma'_2)$ can be reduced to a canonical 6. They are 1) $(++++)$ (D 's to same direction, angle 0°), 2) $(++--)$ (D 's to same direction, angle 180°), 3) $(+++-)$ (D 's away from each other, angle 0°), 4) $(+-+)$ (D 's away from each other, angle 180°), 5) $(-+++)$ (D 's towards each other, angle 0°), 6) $(-++-)$ (D 's towards each other, angle 180°).

¹Note that in the asymptotic limit the situation is simpler because from the expression

$$W = \frac{\sigma_1 x + i\sigma_2 y}{-i\tau\sigma_1\sigma_2 f(r_a)} = \frac{x + i\sigma_1\sigma_2 y}{-i\tau\sigma_2 f(r_a)}$$

one cannot extract τ in order to say whether it describes a Hopfion or an anti-Hopfion.

The time evolution for these cases is as follows. For Cases 1 and 2 the system is in the attractive channel (Figure 7, Movie W1). The Hopfions approach each other, bounce a few times, during which they develop some asymmetry and eventually turn over, join and deform into a $Q = 2$ single ring Hopfion. The four remaining cases 3, 4, 5 and 6 are repulsive: As the Hopfions recede they slowly turn around their axis and it is plausible that they eventually turn enough to attract each other and return to form a single ring state. That is, we know that due to the fact $2 \times 1^{3/4} > 2^{3/4}$ the asymptotically separated configuration is a higher energy state than the single-ring configuration but it is unclear whether the initial configurations for these four repulsive systems have large enough repulsive (escape) energy to form the higher energy state. As the Hopfions quickly reach the border of any finite computational space, this is a hard question to answer using numerical methods alone.

3.3.2 Boundary effects

In order to better understand the effect of boundaries, we considered the $(++--)$ case further and calculated its evolution in physical grids of different size, while keeping the grid constant and boundary conditions unchanged. Our results are given in Movie W2, which combines the result from cubes of physical size 30.00^3 , 45.00^3 , 67.50^3 , and 101.25^3 having 200^3 , 300^3 , 450^3 , and 675^3 grid points, they are located at top left, top right, bottom left and bottom right, respectively.

In all cases the simulation starts with a slight repulsion during which the colors of the isosurfaces rotate towards the same phase. Then the Hopfions approach each other and bounce several times and eventually form a $Q = -2$ un-knot Hopfion.

The difference in the dynamics can be explained by the existence of two competing effects: the fixing of the boundary value to $\phi = (0, 0, -1)$ tends to stabilize the configuration, while the radiation reflecting from the boundaries tends to un-stabilize it. The radiation effects are illustrated in Figure 8, where we have plotted the values of the usually very revealing quantity $(\partial_t \phi)$ on a slice of the box. The box in upper cases is relatively small and the closeness of the fixed boundary stabilizes the situation well and many bounces are required to un-stabilize it, even though there is lots of radiation bouncing around. The fastest un-stabilization occurs with box size 450^3 (lower left), in that case radiation effects overwhelm the boundary stabilization. In the largest box (lower right) the radiation takes a longer time to reach the interaction region and therefore more bounces are again possible before deformations.

Clearly the major difference between these simulation is the time at which the radiation wave of the initial relaxation travels to the boundary and is reflected back to center of the

grid. In smaller grids the boundary is so close that the first reflection happens before the Hopfions even collide the first time. After a few more reflections an interference pattern is formed in the background but it is reasonably symmetric. In the larger grids the first reflected wave passes over the Hopfion pair during the first couple of oscillations and this asymmetric perturbation causes the state to unwind faster. Nevertheless the final result is always the same

3.3.3 Side-by-side Hopfions

Another case considered by Ward is that of Hopfion rings side by side on the x -axis. The ansatz is now

$$W = \frac{\sigma_1(x-a) + i\sigma_2y}{z - i\tau\sigma_1\sigma_2f(r_{x-a})} + \frac{\sigma'_1(x+a) + i\sigma'_2y}{z - i\tau\sigma'_1\sigma'_2f(r_{x+a})}. \quad (7)$$

Here $r_{x\pm a} = ((x \pm a)^2 + y^2 + z^2)^{1/2}$. In this case also the 16 possible sign combinations can be divided into 6 essentially different ones, to which others are related by rotations: 1) (+ + ++), polarization vectors D parallel, 2) (+ + -+), antiparallel, 3) (+ + --), parallel, 4) (- - ++), parallel, 5) (+ + +-), antiparallel, 6) (+ - ++). antiparallel. Cases 3 and 4 (and Cases 5 and 6) are related by an overall sign change, which cannot be generated by a rotation.

Considering Hopfions asymptotically as dipole pairs and studying the forces between them led Ward to introduce the second attractive channel which corresponds to our Case 3 above. Ward's energy minimization gave an axially-symmetric ring for $Q = 2$. This is believed to be the true global static minimum. [29]

Our numerical simulations show that the attractive and repulsive channels yield the same qualitative behavior as in the stacked case. However, now the attractive channel comprises of initial configurations 3, 4, 5, and 6 while the repulsive channel contains 1 and 2. As an example of the attractive channel, we give case 5 in Figure 9, Movie W3).

In order to study the repulsive case further we chose to change somewhat the rotation angle of the initial state. After rotating the second Hopfion by angle θ the ansatz (7) can be written as

$$W = \frac{\sigma_1(x-a) + i\sigma_2y}{z - i\tau\sigma_1\sigma_2f(r_{x-a})} + \frac{\sigma'_1((x+a)\cos\theta + y\sin\theta) + i\sigma'_2(y\cos\theta - (x+a)\sin\theta)}{z - i\tau\sigma'_1\sigma'_2f(r_{x+a})}. \quad (8)$$

As can be seen the dependent variable $r_{x\pm a}$ is invariant under rotation.

Recall that the configurations (+ + +-) and (+ + -+) were respectively in the attractive and repulsive channels. Now let us fix σ configuration to repulsive (+ + -+) with $\theta = 0$, then the attractive (+ + +-) is obtained from (8) with $\theta = 180^\circ$. It has already been observed that even in the repulsive case the Hopfions turn around and could return

if the computational box would be big enough. In order to study a case with only slight repulsion we chose the configuration $(+ + -+)$ for $\theta = 20^\circ$ and found it to be attractive (Figure 11 and Movie W4) while $\theta = 5^\circ$ was still repulsive (Movie W5). Similarly, for states $(+ + --)$ and $(+ + ++)$: $(+ + ++)$ is still repulsive at $\theta = 3^\circ$ but changes to attractive at $\theta = 10^\circ$.

It seems the attractive channels yield qualitatively the same behavior regardless of whether the configuration is stacked or side-by-side and likewise for the repulsive case. The study of the dependence on the initial rotation angle, however, shows that there are quantitative differences, of which we have uncovered one: the repulsive channel contains a different range of initial relative orientations depending on the parameters σ and σ' . This further illustrates the extremely rich set of phenomena associated with Hopfions.

4 Conclusions

Now that we are close to seeing knotted structures in experiments it is important to understand their dynamics. The static knots in the Faddeev-Skyrme model are already well understood and in this paper we have shown that these objects have also dynamically many particle-like properties.

We have here studied the scattering collisions of low charge Hopfions. In general the results show remarkable particle-like behavior. We have verified again their tendency to form bound states, due to the charge-energy dependence $E \sim |Q|^{\frac{3}{4}}$; we have also seen the associated radiation of the released energy. With suitable speeds and impact parameters we can also have grazing scattering, without bound state formation. Since the internal structure of Hopfions is quite complicated the results of the scattering process depend strongly on the initial configuration, and not only on the initial positions and velocities but also on the internal specifics (such as orientation, spin, and relative phase) of the scattering objects[36].

We have also investigated the dynamical stability of static configuration of two stacked or side-by-side unknots discussed by Ward [29]. As expected their evolution depends sensitively on computational aspects due to the mere length of the calculation (due to the initial state being static). The errors arise both from discretizations and in particular from boundary effects of the finite computational box. It seems that the stacked and side-by-side configurations made of two charge 1 Hopfions are all unstable and eventually relax into a charge 2 Hopfion.

Acknowledgments

This work is supported by Academy of Finland grants 47188 and 123311, and by the UK Engineering and Physical Sciences Research Council. The computations were done using the resources provided by the *CSC – IT Center for Science Ltd*, www.csc.fi and by the *M-grid project*, supported by the Academy of Finland, and by *CSC – IT Center for Science Ltd*.

References

- [1] S. L. Sondhi, A. Karlhede, S. A. Kivelson, and E. H. Rezayi. Skyrmions and the crossover from the integer to fractional quantum Hall effect at small Zeeman energies. *Phys. Rev. B*, **47**, 16419–16426 (1993).
- [2] A. Bogdanov. New localized solutions of the nonlinear field equations. *Sov. J. Exp. Theor. Phys. Lett.*, **62**, 247–251 (1995).
- [3] U. K. Rößler, A. N. Bogdanov, and C. Pfleiderer. Spontaneous skyrmion ground states in magnetic metals. *Nature*, **442**, 797–801 (2006).
- [4] S. Mühlbauer, B. Binz, F. Jonietz, C. Pfleiderer, A. Rosch, A. Neubauer, R. Georgii and P. Böni. Skyrmion Lattice in a Chiral Magnet. *Science* **323**, 915–919 (2009).
- [5] X. Z. Yu, Y. Onose, N. Kanazawa, J. H. Park, J. H. Han, Y. Matsui, N. Nagaosa and Y. Tokura, Real-space observation of a two-dimensional skyrmion crystal, *Nature* **465**, 901–904 (2010).
- [6] J.E. Moore, The birth of topological insulators. *Nature* **464**, 194–198 (2010).
- [7] D. Hsieh, *et al.*, Observation of Unconventional Quantum Spin Textures in Topological Insulators. *Science* **323**, 919–922 (2009).
- [8] Y. Xia *et al.*, Observation of a large-gap topological-insulator class with a single Dirac cone on the surface. *Nature Physics*, **5**, 398–402 (2009).
- [9] Y. L. Chen *et al.* Experimental Realization of a Three-Dimensional Topological Insulator, Bi₂Te₃. *Science*, **325** 178–181 (2009).
- [10] J. E. Moore, Y. Ran, X.-G. Wen, Topological Surface States in Three-Dimensional Magnetic Insulators, *Phys. Rev. Lett.* **101**, 186805 (2008).
- [11] W. Thompson (Lord Kelvin), On vortex atoms. *Phil. Mag.* **34**, 15–24 (1867).

- [12] P. Sutcliffe, Vortex rings in ferromagnets: Numerical simulations of the time-dependent three-dimensional Landau-Lifshitz equation. *Phys. Rev. B* **76**, 184439 (2007).
- [13] Y. Kawaguchi, M. Nitta, M. Ueda, Knots in a spinor Bose-Einstein condensate. *Phys. Rev. Lett.* **100**, 180403 (2008).
- [14] M. Dennis, R. King, B. Jack, K. O’Holleran, M. Padgett, *Nature Physics* **6**, 118–121 (2010).
- [15] L.D. Faddeev, “Quantization of solitons” (Princeton preprint IAS-75-QS70, 1975).
- [16] E. Babaev, L. D. Faddeev, A. Niemi, Hidden symmetry and knot solitons in a charged two-condensate Bose system. *Phys. Rev.* **B65**, 100512(R) (2002).
- [17] Ü. Parts *et al.*, Phase diagram of vortices in superfluid ^3He – A. *Phys. Rev. Lett.* **75**, 3320–3323 (1995).
- [18] R. Bott, L. W. Tu, *Differential forms in algebraic topology* (Springer-Verlag, 1982).
- [19] A. F. Vakulenko, L. V. Kapitanskii, Stability of solitons in S^2 in the nonlinear σ -model. *Sov. Phys. Dokl.* **24**, 433 (1979).
- [20] F. Lin, Y. Yang, Existence of energy minimizers as stable knotted solitons in the Faddeev model. *Commun. Math. Phys.* **249**, 273–303 (2004).
- [21] L.D. Faddeev, A. J. Niemi, Stable knot-like structures in classical field theory. *Nature* **387**, 58–61 (1997).
- [22] J. Gladikowski, M. Hellmund Static solitons with non-zero Hopf number. *Phys. Rev.* **D56**, 5194–5199 (1997).
- [23] R.A. Battye, P. Sutcliffe, Solitons, links and knots. *Proc. Roy. Soc. Lond.* **A455**, 4305–4331 (1999).
- [24] R. A. Battye, P. M. Sutcliffe, Knots as stable soliton solutions in a three-dimensional classical field theory. *Phys. Rev. Lett.* **81**, 4798–4801 (1998).
- [25] P. M. Sutcliffe Knots in the Skyrme-Faddeev model. *Proc. Roy. Soc. A* **463**, 3001–3020 (2007).
- [26] J. Hietarinta, P. Salo, Faddeev-Hopf knots: Dynamics of linked un-knots. *Phys. Lett.* **B451**, 60–67 (1999).

- [27] J. Hietarinta, P. Salo, Ground state in the Faddeev-Skyrme model. *Phys. Rev.* **D62**, 081701(R) (2000).
- [28] J. Hietarinta, J. Jäykkä, P. Salo, Relaxation of twisted vortices in the Faddeev-Skyrme model. *Phys. Lett.* **A321**, 324–329 (2004).
- [29] R.S. Ward, The interaction of two Hopf solitons, *Phys. Lett B* **473**, 291-296 (2000).
- [30] R. A. Battye, P. M. Sutcliffe, Skyrmions, fullerenes and rational maps. *Rev. Math. Phys.* **14**, 29–86 (2002).
- [31] M. K. Carpenter, C. A. Kennedy, “Fourth-Order N-Storage Runge-Kutta Schemes” (NASA Technical Memorandum 109112, 1994).
- [32] SAMRAI (Structured Adaptive Mesh Refinement Application Infrastructure) <http://www.llnl.gov/casc/SAMRAI/>
- [33] VisIt: <https://wci.llnl.gov/codes/visit/>
- [34] J. Hietarinta, J. Jäykkä, P. Salo Dynamics of vortices and knots in Faddeev’s model. In Ferreira, A., Gomes, F. & Zimmerman, H. (eds.) *Proceedings of Science (Sissa) PoS(unesp2002)017* (2002).
- [35] D. Harland, M. Speight, and P. Sutcliffe. Hopf solitons and elastic rods. *Phys. Rev.* **D**, **83**, 065008 (2011).
- [36] Further movies will be posted at <http://www.youtube.com/nonlinearUTU>

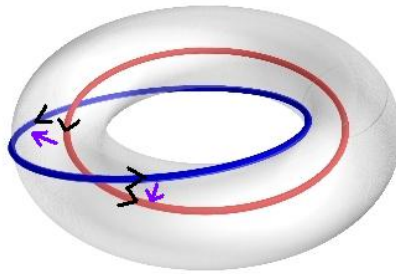


Figure 1: Red line: the preimage of $\phi = (0, 0, +1)$ (vortex core); blue line: the preimage of $\phi = (\frac{3}{4}, 0, \frac{4}{5})$. The lines have been assigned compatible directions and their linking number can then be computed as explained in text.

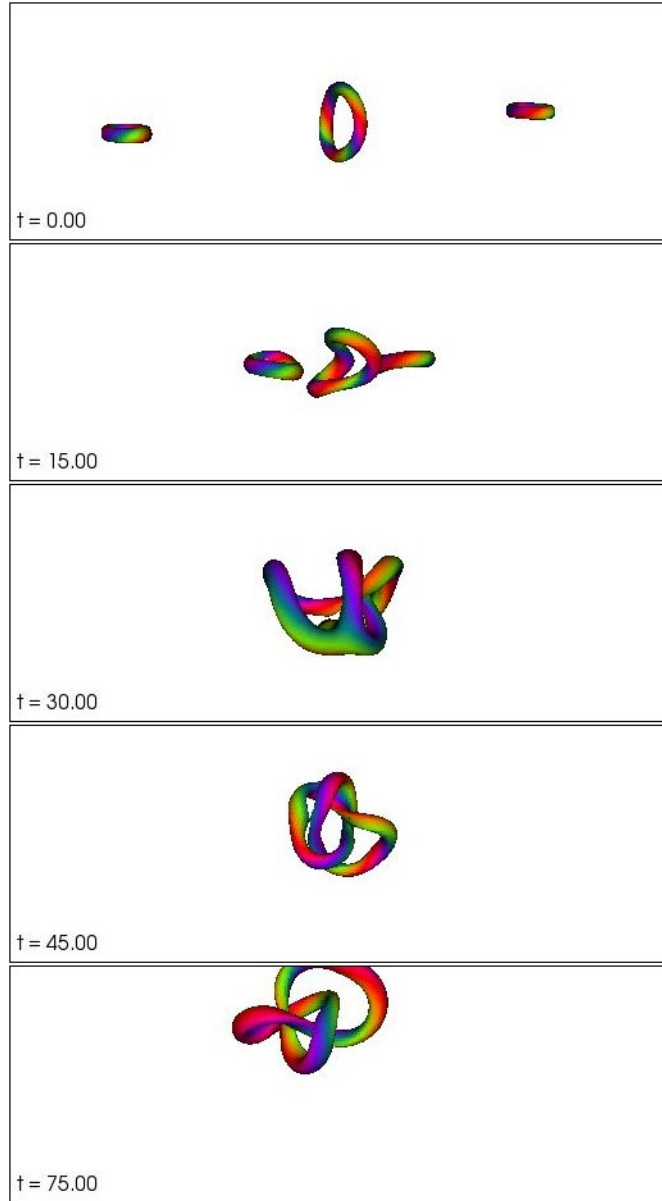


Figure 2: The formation of a trefoil knot by the scattering of two $Q = -2$ Hopfions with velocities ± 0.75 on a stationary $Q = -3$ target. For more details see Movie S1.

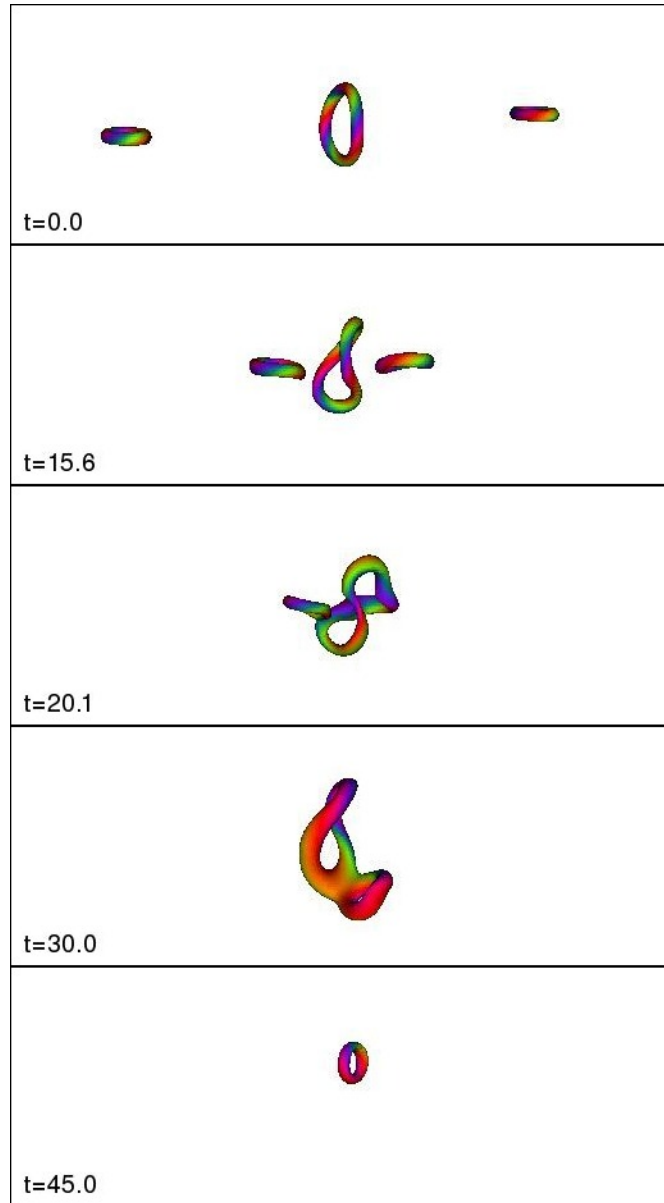


Figure 3: Collision of three Hopfions of charges $Q = -2, +3, -2$ and velocities $0.75, 0, -0.75$, respectively, resulting with a Hopfion of charge -1 . For details see Movie S2.

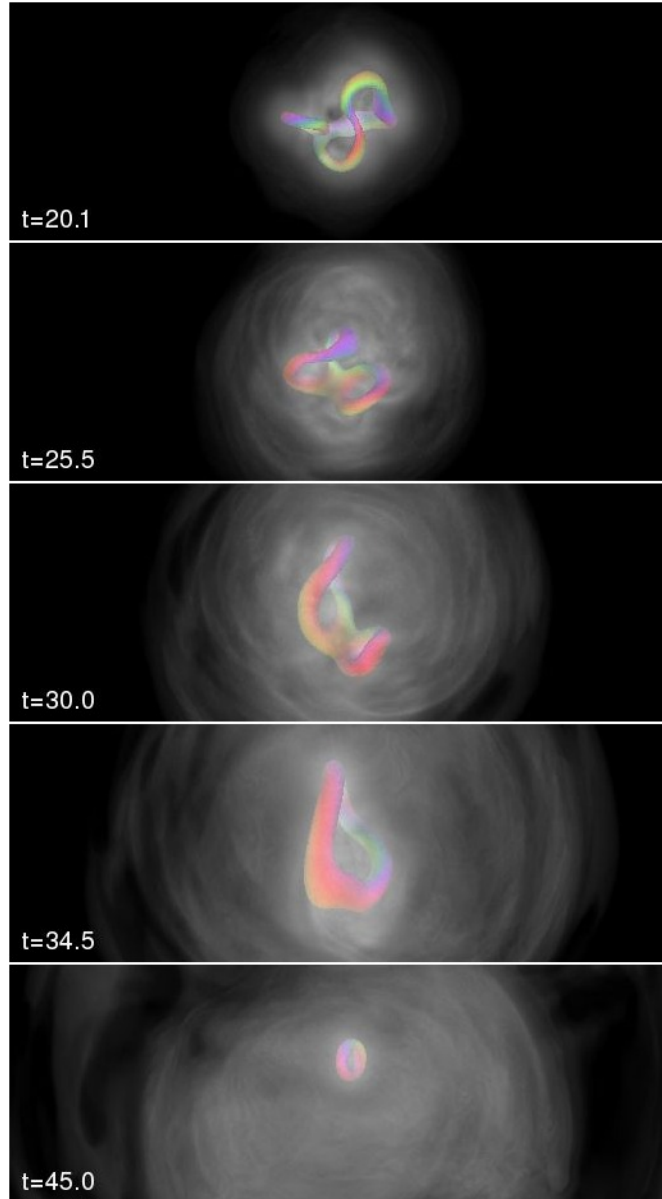


Figure 4: Same scattering process as in Figure 3 but with further intermediate states for the later stage of the deformation process. Here we have added the energy density plot which appears as a grayish halo. See also Movie S3.

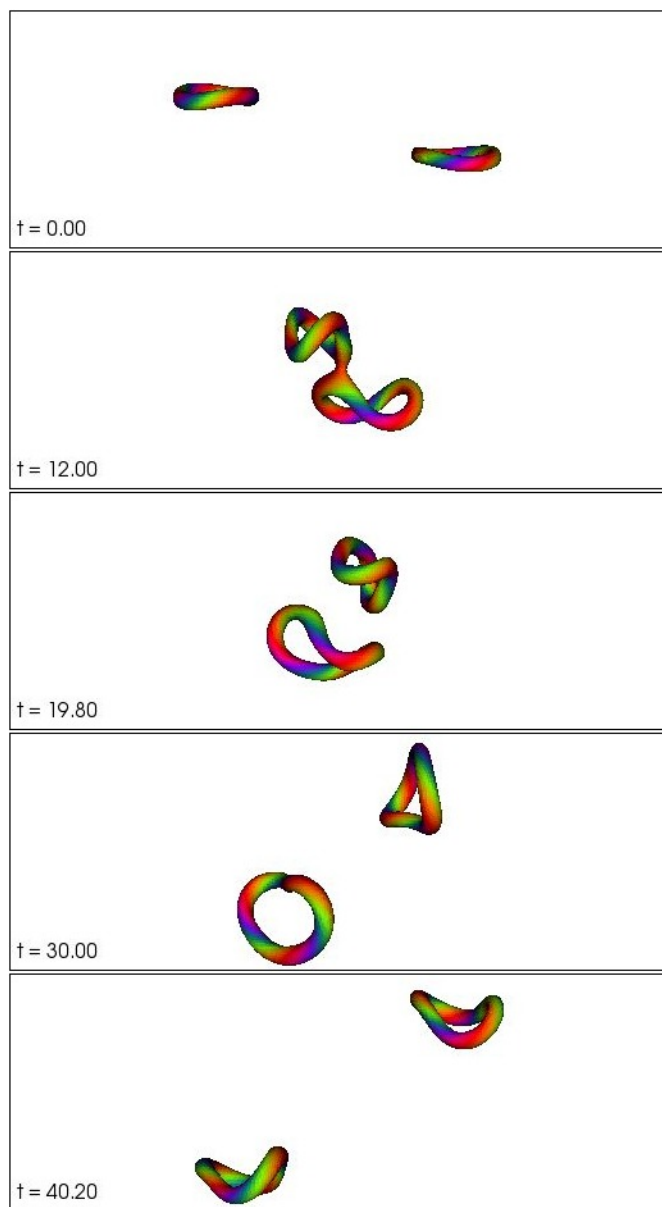


Figure 5: Collision of two Hopfions of charge $Q = -3$. The initial velocities were ± 0.5 and the impact parameter 3.75. For more details see Movie S4.

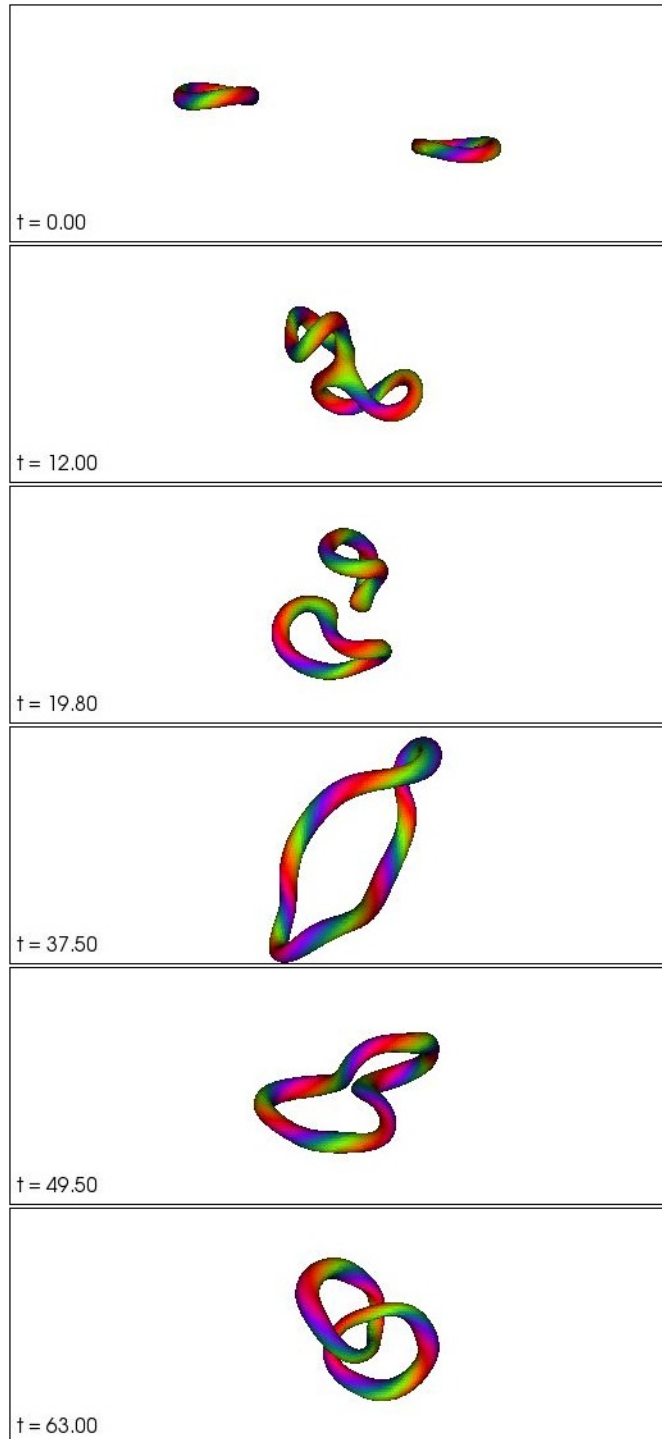


Figure 6: Same as in Figure 5 except that impact parameter is 3.6. For more details see Movie S5.

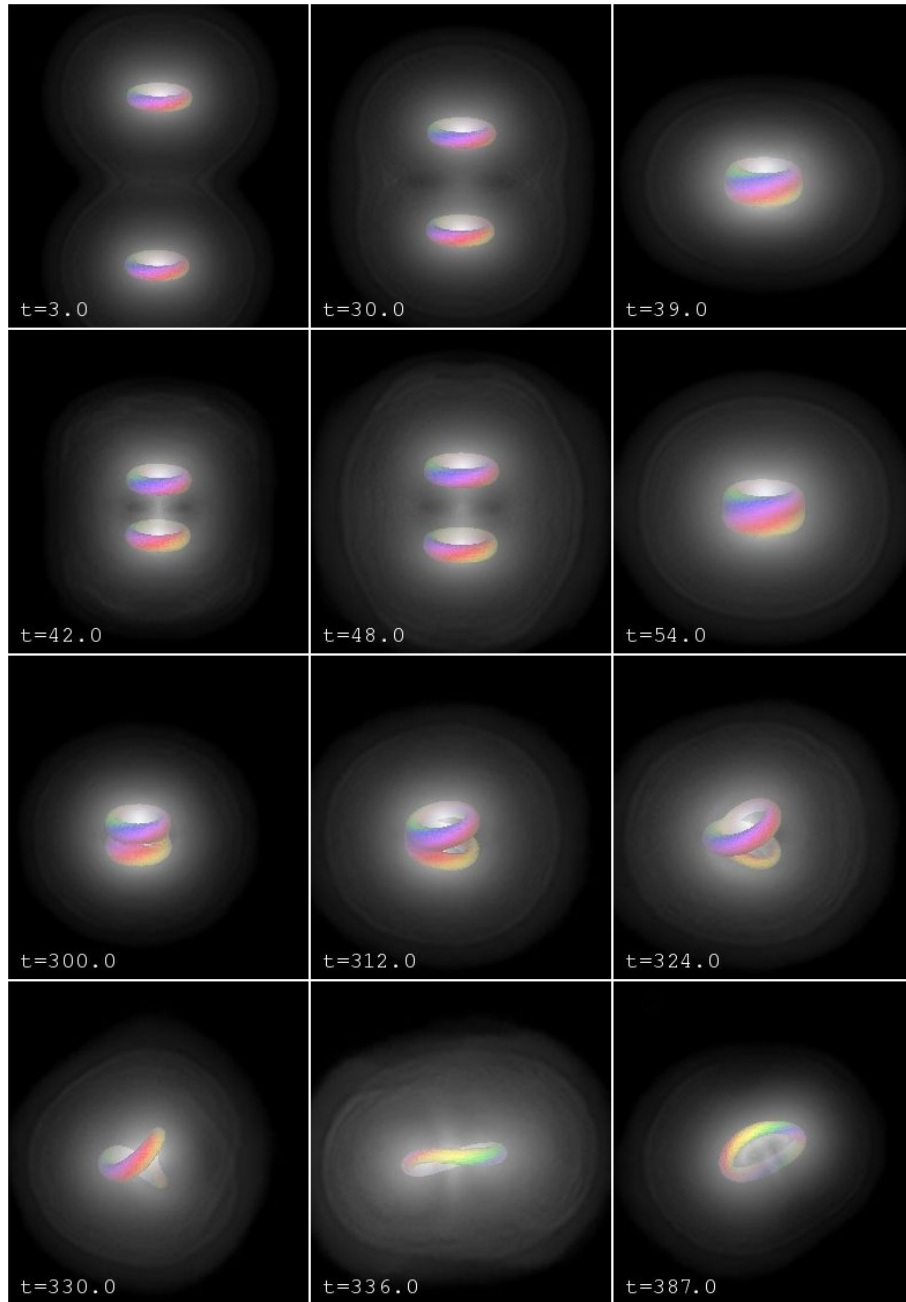


Figure 7: Stacked configuration $(+++)$ produces an attractive interaction between the two $H = 1$ Hopfions. The pair oscillates multiple times before a slight asymmetry brings the system to the more stable $H = 2$ single-ring configuration. For details see Movie W1, and the discussion in the end of section 3.3.1.

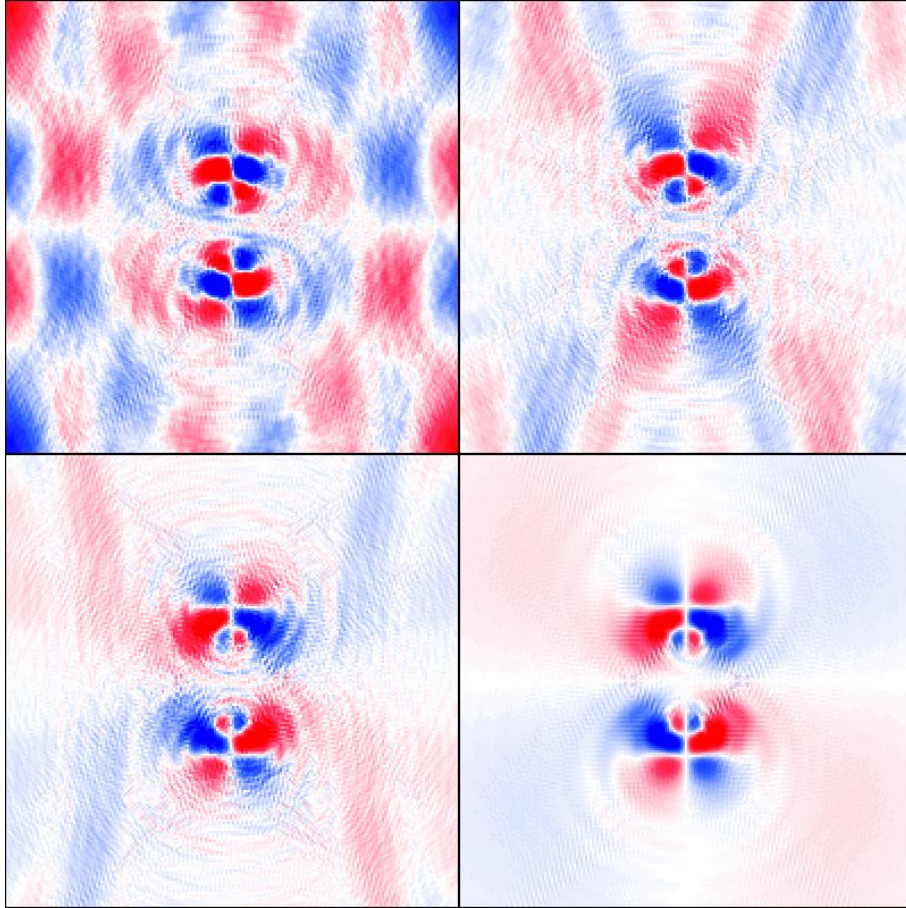


Figure 8: Figure shows four 30^2 slices of the canonical derivative field ψ_2 between a fixed interval $[-0.05, 0.05]$ at the same moment ($t = 60.0$, $\# = 2000$) in different physical size grids. We can see that the boundary effects are strongly present at the area around the Hopfion's core in the first case, just reaching it in the second and third case and still outside the observed area in the fourth case.

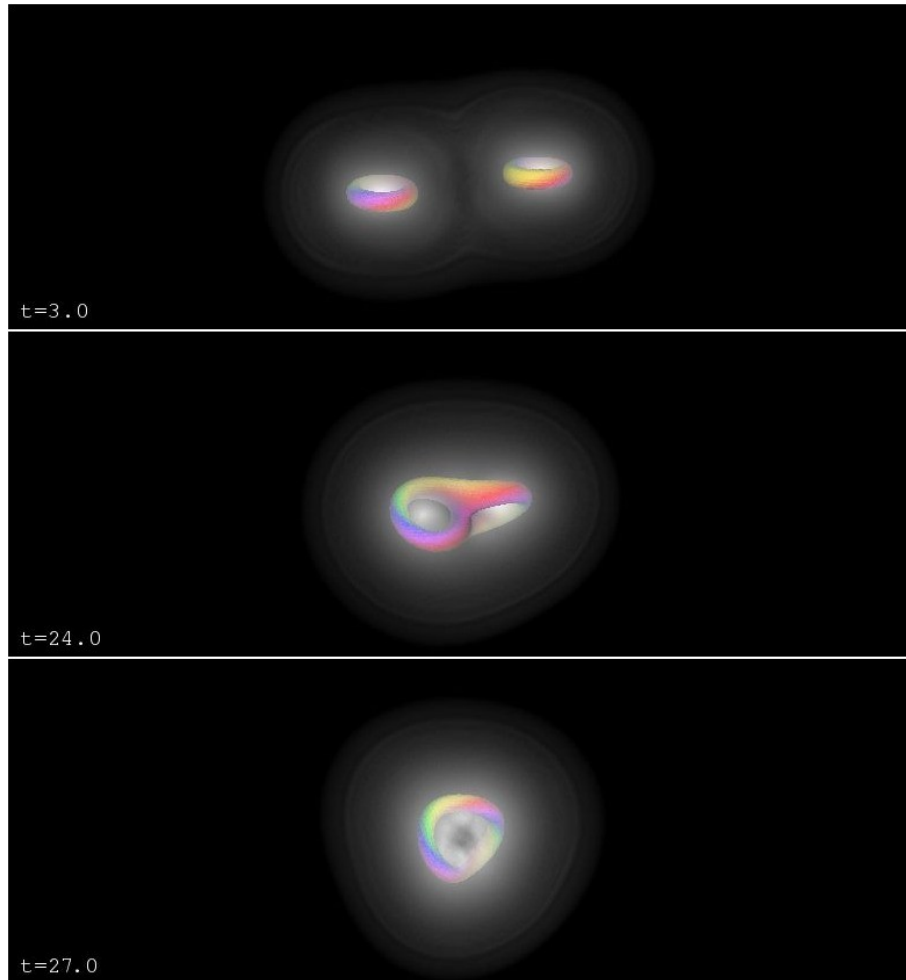


Figure 9: The side-by-side configuration $(+++)$ seems to be attractive without delay and the pair end up in the familiar $H = 2$ single ring configuration. At the end of the simulation the pair oscillates relatively softly having already emitted most of its excess energy. For more detail see Movie W3.

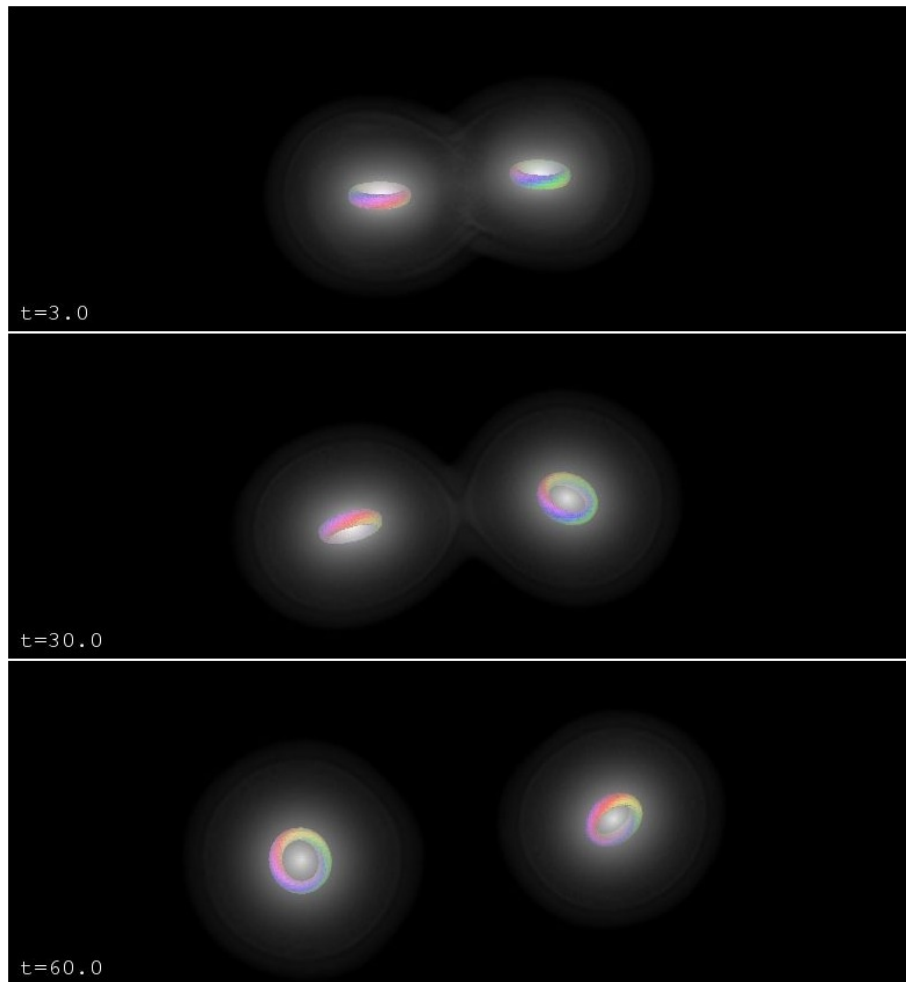


Figure 10: The side-by-side configuration $(+ + - +)$ is repulsive from the start of the simulation and the system end up in the unattached state where the initial Hopfions advance in opposite directions.

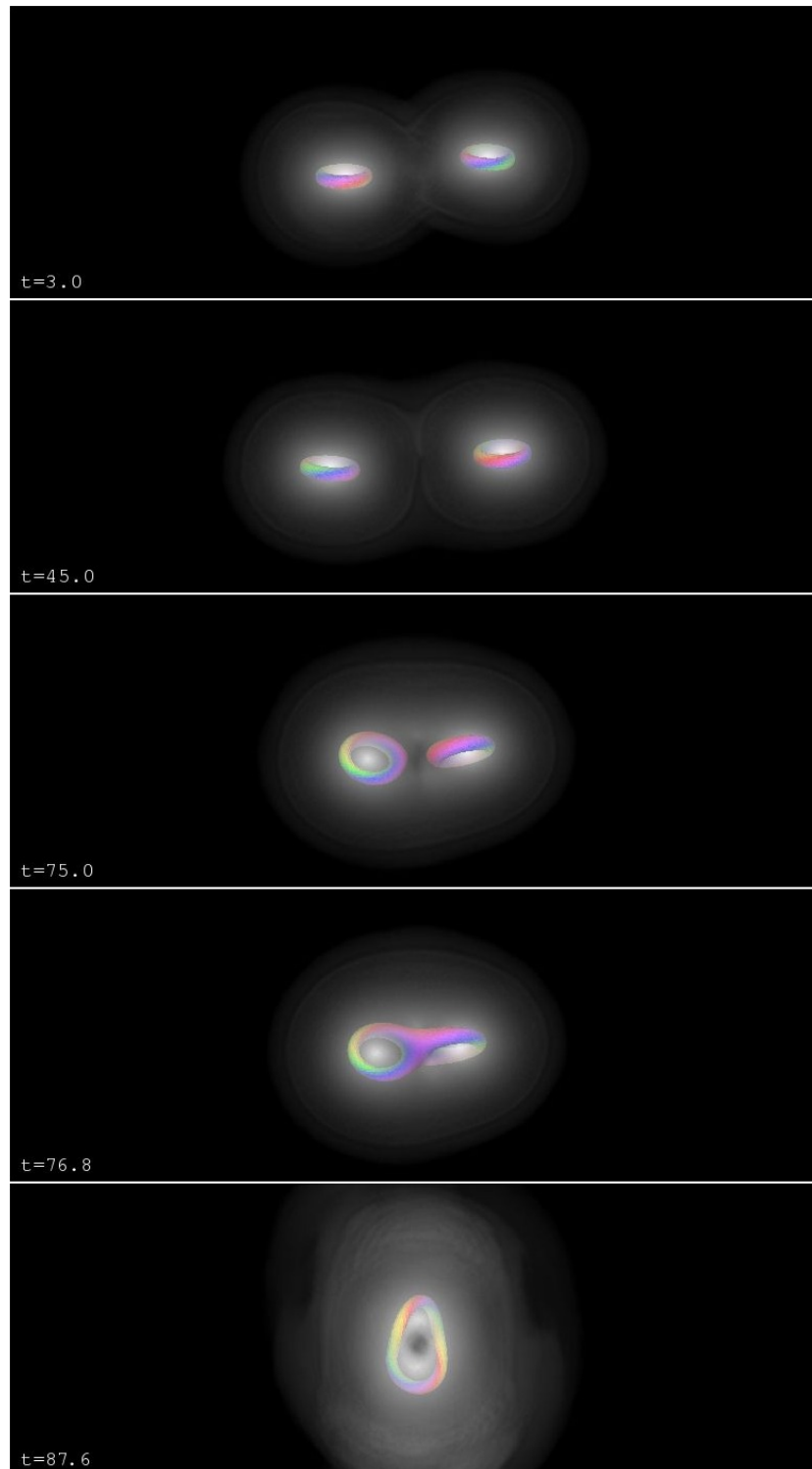


Figure 11: The behavior of the side-by-side system $(++-+)$ changes after a rotation of the second Hopfion by an angle of 20° . Now the Hopfions move further away from each other under a color rotation until the phase difference between them becomes attractive and the single ring configuration $H = 2$ is formed. For more detail see Movie W4).